# Model space diabatization for quantum photochemistry

Shaohong L. Li, Donald G. Truhlar, Michael W. Schmidt, and Mark S. Gordon

Citation: The Journal of Chemical Physics **142**, 064106 (2015); doi: 10.1063/1.4907038
View online: http://dx.doi.org/10.1063/1.4907038
View Table of Contents: http://scitation.aip.org/content/aip/journal/jcp/142/6?ver=pdfcov
Published by the AIP Publishing

# Model space diabatization for quantum photochemistry

Shaohong L. Li,[1] Donald G. Truhlar,[1,a)] Michael W. Schmidt,[2] and Mark S. Gordon[2]
[1]*Department of Chemistry, Chemical Theory Center, and Supercomputing Institute, University of Minnesota, Minneapolis, Minnesota 55455, USA*
[2]*Department of Chemistry, Iowa State University, Ames, Iowa 50011, USA*

(Received 11 November 2014; accepted 19 January 2015; published online 11 February 2015)

Diabatization is a procedure that transforms multiple adiabatic electronic states to a new representation in which the potential energy surfaces and the couplings between states due to the electronic Hamiltonian operator are smooth, and the couplings due to nuclear momentum are negligible. In this work, we propose a simple and general diabatization strategy, called model space diabatization, that is applicable to multi-configuration quasidegenerate perturbation theory (MC-QDPT) or its extended version (XMC-QDPT). An advantage over previous diabatization schemes is that dynamical correlation calculations are based on standard post-multi-configurational self-consistent field (MCSCF) multi-state methods even though the diabatization is based on state-averaged MCSCF results. The strategy is illustrated here by applications to LiH, LiF, and thioanisole, with the fourfold-way diabatization and XMC-QDPT, and the results illustrate its validity. © *2015 AIP Publishing LLC.* [http://dx.doi.org/10.1063/1.4907038]

## I. INTRODUCTION

The Born-Oppenheimer approximation decouples the motion of electrons from that of nuclei in molecular systems, and this leads to the concepts of adiabatic electronic states and potential energy surfaces (PESs). The adiabatic electronic states and their energies are calculated with fixed nuclear positions, and the nuclei move in the potential created by the electrons in a single electronically adiabatic state. This approximation is valid when the electronic states are separated by a large energy gap but breaks down near intersections or avoided crossings where two or more electronic states become close in energy and are consequently closely coupled.[1–3] In this case, the coupling of electronic states by the nuclear momentum vector operators cannot be neglected, and more than one adiabatic electronic state has to be taken into account in the equations of motion for the nuclei. For $N$ atoms, the nuclear momentum couplings, often called nonadiabatic couplings, are $3N$-dimensional vectors that are unsmooth near, and singular at, conical intersections, making them cumbersome to use in dynamics simulations. Nevertheless, by changing the electronic basis from the adiabatic states to so-called diabatic states,[4] it is possible to reduce the magnitude of those vector couplings to be negligible for most purposes.

Sometimes the diabatic states are called "quasi-diabatic" while "diabatic" is reserved for the basis in which the vector couplings strictly vanish, but since strict diabatic states do not exist in general,[5] we—as do many others—simply use the term "diabatic" to refer to bases in which the vector couplings are negligible (or neglected) but do not necessarily vanish. In a diabatic basis, the electronic states are still coupled by the electronic Hamiltonian operator, and the couplings appear as off-diagonal elements of the electronic Hamiltonian matrix, but these couplings, usually called diabatic couplings, are smooth scalars that are relatively easy to use in dynamics calculations and are suitable for analytic representations. Therefore, diabatic bases are preferable to adiabatic basis for many aspects of dynamics calculations.

Diabatic states are not unique, and many methods have been proposed for obtaining them for specific problems;[4,6–31] for example, in some methods, this is done by enforcing the smoothness of some molecular properties. Of special interest are methods applicable to electronic structure calculations that add dynamical correlation to multi-configurational self-consistent field (MCSCF)-type wave functions[32–36] since currently these are the most reliable wave function approximations for describing potential energy surfaces of closely coupled electronic states. The present article is concerned with quasidegenerate perturbation theory (QDPT) methods in which the final step is the diagonalization of a low-dimensional effective Hamiltonian in a model space where the dimension is the number of adiabatic states of interest. The most popular of such methods[37–42] are in principle able to treat several states in a balanced manner and recover a large part of the dynamic correlation with a relatively modest computational cost compared to the more expensive multireference configuration interaction (MRCI) or multireference coupled cluster (MRCC) theories. Examples of such methods are the state-averaged complete active space self-consistent field method (SA-CASSCF) followed by second-order multi-configurational quasi-degenerate perturbation theory (MC-QDPT),[37] extended MC-QDPT (XMC-QDPT),[38] multistate complete active space second-order perturbation theory (MS-CASPT2),[39] extended MS-CASPT2 (XMS-CASPT2),[42] and quasidegenerate second-order $n$-electron valence state perturbation theory (QD-NEVPT2).[40]

The fourfold way[18,19,21,29] is a diabatization method that enforces the smoothness of wave functions by first construct-

a)Email: truhlar@umn.edu

 

ing diabatic molecular orbitals (DMOs) by a threefold density criterion and a sometimes employed fourth criterion based on reference orbitals and then applying a configurational uniformity step originally proposed by Atchity and Ruedenberg.[13,15] The fourfold way was developed to have general applicability to diverse types of electronic states and electronic excitation problems. It was formulated in the context of SA-CASSCF and MC-QDPT, but it is straightforwardly extended to the other QDPT methods mentioned in the previous paragraph. However, as currently formulated, the fourfold way with any of these QDPT theories evaluates second-order perturbation energies in the DMO basis. Although it is possible to formulate QDPT in a way that is invariant to certain transformations of orbitals (see, for example, Ref. 38 for the case of XMC-QDPT), such a reformulation is computationally inefficient and is not implemented in electronic structure packages. In the original paper on applying the fourfold way with MC-QDPT,[19] we pointed out the dependence of MC-QDPT energies on orbital rotations, and we resolved the ambiguity by defining the adiabatic energies as those calculated using the DMOs rather than the canonical molecular orbitals (CMOs). In the original work and subsequent work[26,43–48] we found, when we checked, only small differences between the two sets of adiabatic energies; however, for a current application to thioanisole, we found differences of up to 0.8 eV when using DMOs obtained by the fourfold way and up to 0.05 eV when using DMOs obtained by the threefold way. Therefore, we developed the scheme presented here to give a diabatic potential energy matrix that, when diagonalized, gives precisely the adiabatic energies of standard QDPT with CMOs.

The diabatization strategy for MC-QDPT and XMC-QDPT (denoted collectively as (X)MC-QDPT) developed here is called model space diabatization (MSD). It utilizes information from an initial CASSCF-level diabatization and a standard QDPT calculation to perform a final diabatization at the QDPT level. In this paper, we will use the fourfold-way diabatization at the CASSCF level and the XMC-QDPT method to demonstrate the strategy, but by construction, MSD can also be applied with other diabatization schemes[30,49] or other MCSCF-type wave functions[41] for the initial diabatization step. As will be shown later, the MSD scheme requires that the MCSCF-level diabatization generates diabatic states that span the same space as do the MCSCF adiabatic states for the subset of states being considered, but its formulation does not involve the details of the MCSCF-level diabatization. All information needed for MSD is already generated by the MCSCF-level diabatization and by standard QDPT calculations, and the additional calculations only involve elementary matrix algebra like multiplication and transpose, whose computational cost and complexity are negligible compared to the MCSCF and QDPT steps.

To test the new strategy, we choose three challenging test cases, namely, the potential energy curves of the ground and excited states of LiH, LiF, and thioanisole. These systems all have state crossings and are challenging because the positions of the crossings are sensitive to dynamical correlation; thus the crossings occur at quite different places for MCSCF and QDPT. To give the reader an example, Fig. 1 shows the potential energy curves of the three lowest $^1\Sigma^+$ states of LiF

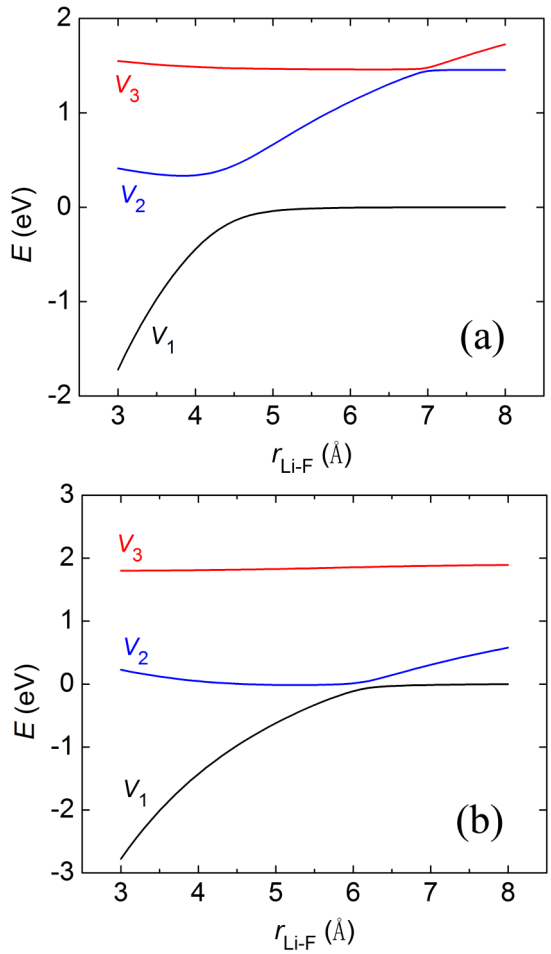


FIG. 1. Adiabatic ($V_1 - V_3$) potential energy curves of LiF as functions of the internuclear separation as calculated by (a) SA-CASSCF and (b) XMC-QDPT.

as calculated by SA-CASSCF and XMC-QDPT. (The details of the calculations will be given later.) The difference of the positions of the avoided crossings is clear, and this poses the question of whether the new strategy can account for such a shift of state crossings while keeping the potential curves smooth, especially in the intermediate region between the two state crossing locations.

The present article is about using model space quantities in certain steps of the generation of diabatic states. As such, it is not a paper about the fourfold way per se. Nevertheless, our examples use the fourfold way, and hence, some discussion of the fourfold way is useful as background. Some steps of the fourfold way are automatic, but others are not. The fourfold way produces DMOs, which are smoothly varying, and then the transformation of the usual configuration state functions (CSFs) written in terms of canonical (adiabatic) MOs into orthogonal diabatic CSFs (CSFs written in terms of DMOs) is unique. Next, one must specify the diabatic prototype CSFs that produce smooth diabatic states. The choice of diabatic prototypes near the equilibrium geometry usually corresponds to what one would expect on the basis of a valence bond analysis (for example, distinguishing a valence excitation from a charge transfer one) or other conventional way of classifying the character of the states (for example,

distinguishing an $n \rightarrow \pi^*$ excitation from a $\pi \rightarrow \pi^*$ one), but every molecule is different and has its own nuances so no general prescription can be given. Ideally, one would need only one diabatic prototype per diabatic state, but in practice, one obtains smoother results if one adds some dominating correlating configurations to the diabatic prototype lists. Once the diabatic prototypes are specified, the method becomes automatic, and it generates orthogonal diabatic state functions. The resulting diabatic states will depend, to some extent, on the choice of reference orbitals (if needed) in the fourth term of the DMO generation and on the choice of diabatic prototypes in the CSF transformation step, but if the choices made are physically correct, the various results should be qualitatively similar; the lack of uniqueness was already mentioned in an earlier paragraph and is a well known issue in generating diabatic states, i.e., unique diabatic states do not exist because strictly diabatic states do not exist. An instructive analogy is with multiconfiguration self-consistent-field calculations, such as CASSCF and RASSCF. CASSCF results depend quantitatively on the choice of active space, and RASSCF results also depend quantitatively on the restrictions, but in either case—if one makes physical choices—the various results should be qualitatively similar. For a dissociation process, the diabatic states might (but need not) correspond to the lowest energy states at an asymptote. For example, in an alkali hydride or alkali halide, one clearly has a mixture of ionic and covalent states at equilibrium, but the ionic diabatic state might cross several covalent states between equilibrium and dissociation. In some experiments, the actual production of ionic dissociated states might be energetically forbidden, but a diabatic treatment of the photodissociation to produce various neutral excited states will nevertheless require one to have an ionic state included in the diabatic state list.

The present paper uses example of conical intersections where two adiabatic states intersect. In general, one expects that there are also points of confluence of three or more potential energy surfaces.[1] Although the method presented here would be expected to be valid also for such cases, we limit explicit discussion to the intersection of just two states.

The rest of the paper is organized as follows. In Secs. II A and II B, we will review the fourfold-way diabatization and the relevant theoretical aspects of (X)MC-QDPT (the differences between MC-QDPT and XMC-QDPT have no effect on the procedures, so we can discuss them both at the same time). Section II C then introduces the MSD strategy and the detailed algorithm for calculations. Section III presents the computational details of three test cases, namely, LiH, LiF, and thioanisole, and Sec. IV presents the results and discussion. Section V gives a summary.

## II. THEORY

### A. Review of the fourfold way

The fourfold way[18,19,21,29] is a general diabatization scheme based on configurational uniformity that generates diabatic states spanning the same model space as the selected adiabatic states; the diabatic states and the adiabatic states are related by an orthogonal transformation. The fourfold way was first formulated at the CASSCF level[18] and then extended to the MC-QDPT level[19] and to include spin-orbit coupling.[45] At the MC-QDPT level, it can be used with diabatic molecular orbitals obtained at either the MC-QDPT level[19] or the CASSCF level.[29] It has been successfully applied to a variety of systems at both the CASSCF and MC-QDPT levels.[26,43–48] However, as mentioned in the Introduction, for some cases, the original fourfold way at the MC-QDPT level may give results that are quite different from the standard MC-QDPT method. These problematic cases are the motivation for developing the present MSD strategy.

The fourfold way generates diabatic states that are smooth and retain their valence character for all molecular geometries of interest; it accomplishes this by means of configurational uniformity. In particular, the "valence character" of a diabatic state is determined by a group of CSFs called diabatic prototypes of which at least one is dominant at each molecular geometry of interest, with the requirement that the diabatic prototype groups corresponding to different diabatic states cannot have any CSFs in common. For the many-electron CSFs to be smooth functions of geometry, they must be expressed in terms of smoothly varying one-electron molecular orbitals (MOs), but the CMOs generated by SA-CASSCF or indeed by any variational procedure often change character due to avoided crossings and so are not suitable for this purpose. The first step of the fourfold-way diabatization is therefore to generate smoothly varying MOs, which are called DMOs. We next review the procedure for obtaining DMOs from SA-CASSCF wave functions.

In the inactive and external orbital spaces, the DMOs are identical to CMOs since these orbitals are doubly occupied or unoccupied in all the "internal" CSFs (CSFs generated by distributing all active electrons in all active orbitals in all possible ways, from which the CASSCF wave functions are constituted) and thus inconsequential in characterizing the internal CSFs. In the active orbital space, the DMOs are obtained by an orthogonal transformation of the CMOs so that they satisfy the "threefold density criterion" and, if needed, the "maximum overlap of reference MOs" (MORMO) criterion.

The threefold density criterion is to maximize the following functional of the orbitals:

$$D_3 = \alpha_N D^{NO} + \alpha_R D^{ON} + \alpha_T D^{TD}, \quad (1)$$

where $D^{NO}$, called the natural orbital term, measures how close the MOs are to state-averaged natural orbitals; $D^{ON}$, called the occupation number term, is the sum of the diagonal elements of the one-particle density matrix of all the states; and $D^{TD}$, called the transition density term, is related to the transition density matrix. The $D_3$ functional is the weighted average of these three functionals of the orbitals with the weights usually taken as $\alpha_N = 2$, $\alpha_R = 1$, and $\alpha_T = 0$–$0.5$. The threefold density criterion with these particular weights is shown[18] to generate satisfactory DMOs in many situations, but there are difficult cases that require an additional criterion, the MORMO criterion. The reference orbitals for the MORMO criterion can be obtained in two ways. One way is to choose a reference geometry at which the adiabatic states are already approximately equal to the desired diabatic states and use the threefold density criterion to obtain preliminary DMOs, from

which a subset of $\lambda$ DMOs is chosen as reference orbitals. Another way is to use appropriately modified CMOs at a reference geometry, where the modification would typically be to drop some components on all but one center. At any geometry other than the reference geometry, $\lambda$ DMOs are constructed by maximizing a functional related to a generalized "overlap" with the reference DMOs. The rest of the DMOs are constructed by the threefold density criterion.

After the DMOs are generated, complete active space configuration interaction (CAS-CI) calculations are carried out in the DMO basis. These calculations give the same wave functions and energies as CASSCF calculations in the CMO basis. Dominant CSFs for each state are identified at one or several key geometries and are grouped into diabatic prototype groups. Finally, diabatic states at the CASSCF level are constructed by maximizing the preponderance of one of the CSFs in each of the diabatic prototype groups in one or another of the diabatic CSFs. For diabatization at the MC-QDPT level, one performs MC-QDPT calculations in the DMO basis (either the CASSCF DMO basis or a new DMO basis determined at the MC-QDPT level) and diabatizes the MC-QDPT wave functions in the same manner.

In this paper, the calculations of fourfold way diabatization at the XMC-QDPT level use only the CASSCF DMO basis since this basis gives smoother diabatic potentials.[29]

### B. Analysis of the (X)MC-QDPT wave functions

In this paper, we use Granovsky's XMC-QDPT,[38] which is an extension of Nakano's original MC-QDPT.[37] The XMC-QDPT and MC-QDPT differ in the choice of the zero-order Hamiltonian. Granovsky showed that XMC-QDPT gives smoother potential energy surfaces than MC-QDPT. However, the choice of zero-order Hamiltonian is irrelevant to the construction and analysis of our MSD strategy, and hence, we outline here only the relevant theoretical framework shared by XMC-QDPT and MC-QDPT (denoted together as (X)MC-QDPT) and give an analysis of the wave functions. For more details, we refer the readers to the original papers.[37,38,50]

In (X)MC-QDPT, the zero-order wave function space is partitioned into three parts: the $P$ space including all CASSCF states of immediate interest (also called the model space in this article), the $O$ space consisting of the other CASSCF states, and the $S$ space consisting of CSFs that have excitations out of the active space (known as external CSFs). The $P$ and $O$ spaces together form the CAS-CI space ($R$ space) spanned by the CSFs with active electrons distributed among the active orbitals (known as internal CSFs). (The $P$, $O$, $S$, and $R$ spaces were denoted $P_0$, $P_1$, $Q$, and $P$, respectively, in Ref. 19.) The $O$ and $S$ spaces together form the $Q$ space complementary to the $P$ space. The zero-order wave functions are chosen to be the CASSCF states in the $R$ space and the individual external CSFs in the $S$ space. The corresponding partitioning of the electronic Hamiltonian matrix in the basis of zero-order wave functions is illustrated in Fig. 2, following Ref. 38.

The (X)MC-QDPT method uses a unitary transformation $\mathbf{G}$ to block-diagonalize the electronic Hamiltonian $\mathbf{H}$ in the basis of zero-order wave functions

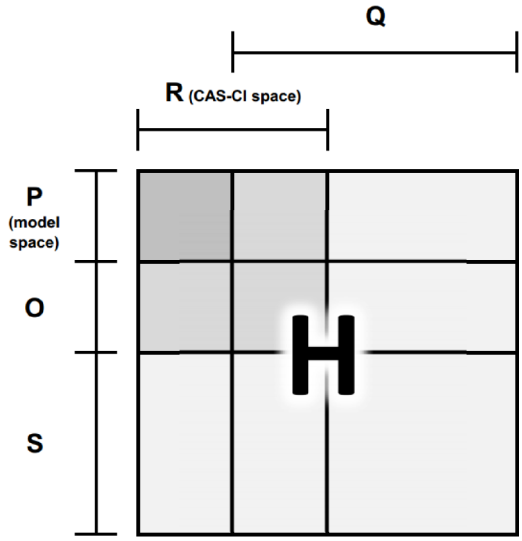


FIG. 2. Schematic of the partitioning of the electronic Hamiltonian matrix into blocks corresponding to subspaces of the wave function space (see the text for an explanation of the notation).

$$\mathbf{G}^{-1}\mathbf{H}\mathbf{G} = \tilde{\mathbf{H}}. \tag{2}$$

Here, $\tilde{\mathbf{H}}$ is a block-diagonal matrix whose $PQ$ and $QP$ blocks are zero; the $QQ$ block is not of interest, and the $PP$ block is defined as the effective Hamiltonian matrix, $\mathbf{H}^{\text{eff}}$. Upon left-multiplication of both sides of Eq. (2) by $\mathbf{G}$, it can be written as

$$\begin{pmatrix} \mathbf{H}_{PP} & \mathbf{H}_{PQ} \\ \mathbf{H}_{QP} & \mathbf{H}_{QQ} \end{pmatrix}\begin{pmatrix} \mathbf{G}_{PP} & \mathbf{G}_{PQ} \\ \mathbf{G}_{QP} & \mathbf{G}_{QQ} \end{pmatrix} = \begin{pmatrix} \mathbf{G}_{PP} & \mathbf{G}_{PQ} \\ \mathbf{G}_{QP} & \mathbf{G}_{QQ} \end{pmatrix}\begin{pmatrix} \mathbf{H}^{\text{eff}} & \mathbf{0} \\ \mathbf{0} & \tilde{\mathbf{H}}_{QQ} \end{pmatrix}, \tag{3}$$

where each block is a rectangular matrix. Diagonalization of $\mathbf{H}^{\text{eff}}$ gives eigenvectors and eigenvalues of $\mathbf{H}^{\text{eff}}$ as well as of $\tilde{\mathbf{H}}$. For the $i$th eigenvector, we have

$$\begin{pmatrix} \mathbf{H}^{\text{eff}} & \mathbf{0} \\ \mathbf{0} & \tilde{\mathbf{H}}_{QQ} \end{pmatrix}\begin{pmatrix} \mathbf{m}_{P,i} \\ \mathbf{0} \end{pmatrix} = \begin{pmatrix} \mathbf{H}^{\text{eff}}\mathbf{m}_{P,i} \\ \mathbf{0} \end{pmatrix} = E_i\begin{pmatrix} \mathbf{m}_{P,i} \\ \mathbf{0} \end{pmatrix}, \tag{4}$$

where $\mathbf{m}_{P,i}$ is a column vector of the same dimension as the $P$ space; $\mathbf{m}_{P,i}$ is an eigenvector of $\mathbf{H}^{\text{eff}}$, and we will call it a "model state"; $E_i$ is the corresponding eigenvalue. By right-multiplying Eq. (3) by the model state, we have

$$\begin{aligned} &\begin{pmatrix} \mathbf{H}_{PP} & \mathbf{H}_{PQ} \\ \mathbf{H}_{QP} & \mathbf{H}_{QQ} \end{pmatrix}\begin{pmatrix} \mathbf{G}_{PP} & \mathbf{G}_{PQ} \\ \mathbf{G}_{QP} & \mathbf{G}_{QQ} \end{pmatrix}\begin{pmatrix} \mathbf{m}_{P,i} \\ \mathbf{0} \end{pmatrix} \\ &= \begin{pmatrix} \mathbf{G}_{PP} & \mathbf{G}_{PQ} \\ \mathbf{G}_{QP} & \mathbf{G}_{QQ} \end{pmatrix}\begin{pmatrix} \mathbf{H}^{\text{eff}} & \mathbf{0} \\ \mathbf{0} & \tilde{\mathbf{H}}_{QQ} \end{pmatrix}\begin{pmatrix} \mathbf{m}_{P,i} \\ \mathbf{0} \end{pmatrix} \\ &= E_i\begin{pmatrix} \mathbf{G}_{PP} & \mathbf{G}_{PQ} \\ \mathbf{G}_{QP} & \mathbf{G}_{QQ} \end{pmatrix}\begin{pmatrix} \mathbf{m}_{P,i} \\ \mathbf{0} \end{pmatrix} \end{aligned} \tag{5a}$$

which yields

$$\begin{pmatrix} \mathbf{H}_{PP} & \mathbf{H}_{PQ} \\ \mathbf{H}_{QP} & \mathbf{H}_{QQ} \end{pmatrix}\begin{pmatrix} \mathbf{G}_{PP}\mathbf{m}_{P,i} \\ \mathbf{G}_{QP}\mathbf{m}_{P,i} \end{pmatrix} = E_i\begin{pmatrix} \mathbf{G}_{PP}\mathbf{m}_{P,i} \\ \mathbf{G}_{QP}\mathbf{m}_{P,i} \end{pmatrix}. \tag{5b}$$

Thus, we see that $E_i$ is also an eigenvalue of the Hamiltonian matrix $\mathbf{H}$ in the chosen (finite) basis of zero-order wave

functions. According to Eq. (5b), the eigenvector of the effective Hamiltonian, $\mathbf{m}_{P,i}$, and the (X)MC-QDPT wave function (eigenvector of $\mathbf{H}$), $\psi_i$, are related by

$$\psi_i = \begin{pmatrix} \mathbf{G}_{PP}\mathbf{m}_{P,i} \\ \mathbf{G}_{QP}\mathbf{m}_{P,i} \end{pmatrix}. \tag{6}$$

Recalling that the $Q$ space is composed of $O$ and $S$ spaces, we can rewrite Eq. (6) as

$$\psi_i = \begin{pmatrix} \mathbf{G}_{PP}\mathbf{m}_{P,i} \\ \mathbf{G}_{OP}\mathbf{m}_{P,i} \\ \mathbf{G}_{SP}\mathbf{m}_{P,i} \end{pmatrix}. \tag{7}$$

In (X)MC-QDPT at the second order, as implemented in the GAMESS[51] electronic structure software package and as we use it here, $\mathbf{G}_{PP}$ is unity and the $\mathbf{G}_{OP}$ part of $\mathbf{G}_{QP}$ is zero,[37] so Eq. (7) becomes

$$\psi_i = \begin{pmatrix} \mathbf{m}_{P,i} \\ \mathbf{0} \\ \mathbf{G}_{SP}\mathbf{m}_{P,i} \end{pmatrix}. \tag{8}$$

Note that all components of $\mathbf{G}_{SP}\mathbf{m}_{P,i}$ are in the $S$ space, and therefore, all components of $\psi_i$ in the CAS-CI space are from $\mathbf{m}_{P,i}$. This means the model states are the projection of the (X)MC-QDPT wave functions on the CAS-CI space at the second order of perturbation. This is the key relationship to be exploited by our proposed model space diabatization strategy.

### C. The MSD strategy

#### 1. Notation

In a given basis, e.g., the zero-order wave functions described above or the individual CSFs, an adiabatic or diabatic wave function can be expressed as a column vector. For example, in the CSF basis, a wave function can be written as

$$|v\rangle = \sum_{\mu=1}^{N^{\mathrm{CSF}}} v_\mu |\mathrm{CSF}_\mu\rangle, \tag{9}$$

where $N^{\mathrm{CSF}}$ is the number of CSFs. A vector $\mathbf{v}$ with components $v_\mu$ can be used to represent this wave function. Hereafter, in this section, we use collections of such vectors $\{\mathbf{v}_i\}$ ($i$ runs from 1 to the number of states) to represent the adiabatic and diabatic states without explicit reference to the basis.

The CASSCF diabatic states $\{\mathbf{d}_i\}$ are given by an orthogonal transformation of the CASSCF adiabatic states of interest $\{\mathbf{c}_i\}$. This transformation is denoted $\mathbf{B}^{\mathrm{CD}}$, and we have

$$\mathbf{d}_i = \sum_{j=1}^{N} \mathbf{c}_j B_{ji}^{\mathrm{CD}}, \tag{10}$$

where $N$ is the dimension of the model space. The (X)MC-QDPT model states $\{\mathbf{m}_i\}$ (representing the same wave functions as the $\mathbf{m}_{P,i}$ in Sec. II B) are also obtained by orthogonally transforming the CASSCF states, and the transformation is denoted $\mathbf{B}^{\mathrm{CM}}$,

$$\mathbf{m}_i = \sum_{j=1}^{N} \mathbf{c}_j B_{ji}^{\mathrm{CM}}. \tag{11}$$

Its inverse transformation, $\mathbf{B}^{\mathrm{MC}}$, that converts the model states to CASSCF states, is the transpose of $\mathbf{B}^{\mathrm{CM}}$,

$$\mathbf{B}^{\mathrm{MC}} = \left(\mathbf{B}^{\mathrm{CM}}\right)^{\mathrm{T}}. \tag{12}$$

All of the transformations are represented by $N \times N$ orthogonal matrices.

#### 2. The MSD strategy applied with fourfold-way diabatization and (X)MC-QDPT

To diabatize the (X)MC-QDPT states within the framework of configurational uniformity, we seek a transformation of the wave functions given by Eq. (8) such that each diabatic state thus generated has the largest projection on the configuration space of a specific diabatic prototype group, i.e., that it is dominated by the configurations of this group; the equations for such a transformation are given by Atchity and Ruedenberg.[15] The prototype groups for (X)MC-QDPT diabatic states are taken to be the same as for CASSCF diabatic states. Therefore, only the components of the wave functions in the CAS-CI space are relevant for the diabatization. Diabatizing the QDPT wave functions (Eq. (8)) is equivalent to diabatizing the model states, resulting in the same transformation. Since the model states span the same $N$-dimensional model space as the selected CASSCF adiabatic states, diabatization of the CASSCF states and of the model states will result in exactly the same diabatic states. From these discussions, we conclude that diabatic states obtained by configurational uniformity from the (X)MC-QDPT wave functions are equivalent *within the CAS-CI space* to the diabatic states obtained from the CASSCF wave functions.

By virtue of this conclusion, the transformation from the (X)MC-QDPT wave functions to the QDPT diabatic states, $\mathbf{B}^{\mathrm{MD}}$, is exactly the same as the transformation from the model states to the CASSCF diabatic states. Such a transformation is equivalent to first transforming the model states back to CASSCF states and then transforming the CASSCF states to the diabatic states

$$\mathbf{B}^{\mathrm{MD}} = \mathbf{B}^{\mathrm{MC}}\mathbf{B}^{\mathrm{CD}}. \tag{13}$$

The diabatic electronic Hamiltonian $\mathbf{U}$ (which is the potential energy matrix governing nuclear motions) is given by similarity-transforming the diagonal adiabatic potential energy matrix $\mathbf{V}$ whose diagonal elements are the (X)MC-QDPT energies

$$\mathbf{U} = \left(\mathbf{B}^{\mathrm{MD}}\right)^{\mathrm{T}}\mathbf{V}\mathbf{B}^{\mathrm{MD}}, \tag{14}$$

where $\mathbf{B}^{\mathrm{MD}}$ is an orthogonal matrix (unitary matrix if we were using a complex treatment). All the necessary ingredients (the matrices $\mathbf{B}^{\mathrm{MC}}$, $\mathbf{B}^{\mathrm{CD}}$, and $\mathbf{V}$) are standard outputs of the CASSCF-level fourfold way and the (X)MC-QDPT calculations. Additional calculations are simply matrix multiplication and transposes.

Although in this paper we discuss and apply the MSD method with the fourfold way and (X)MC-QDPT, by construction, it can also be used with other MCSCF-level diabatization and other QDPT methods if they produce the corresponding $\mathbf{B}^{\mathrm{MC}}$ and $\mathbf{B}^{\mathrm{CD}}$ matrices. This is equivalent to the requirement that the MCSCF-level diabatization and the QDPT generate diabatic states and model states that span the same space as do the MCSCF adiabatic states.

### 3. Consistency of the phases of wave functions

The consistency of the phases of wave functions is an important technical issue that has to be handled carefully when the strategy is applied to potential energy surfaces. Any procedure that generates consistent phases would be acceptable, and the best scheme probably depends on the particular problem (for example, whether the system has an even or odd number of electrons) and on the software used. In the rest of this section, we discuss the general problem and present one scheme (the one we used for the applications in this paper) for ensuring consistent phases.

The wave functions are defined up to a phase factor $e^{i\theta}$, which is ±1 for almost all practical calculations where the wave functions are taken to be real. Accordingly, the signs of the rows and columns of the transformation matrices depend on the phases of both the wave functions being transformed and the transformed wave functions. Although the absolute phases are arbitrary, it is essential for calculating dynamics that the phases be defined consistently from point to point. In general, one can determine the phase along a path through coordinate space (for example, along a trajectory) by enforcing continuity of the signed matrix elements as a function of coordinate change. This strategy is general and applies to the case of either an even or an odd number of electrons.

In addition to the consistency of phases across different geometries, there is consistency of a different type that is more challenging to maintain, namely the consistency of the implicit phases of wave functions in the different matrices at the same geometry. In particular, the MSD strategy concatenates two transformations obtained from two separate calculations, namely, $\mathbf{B}^{\mathrm{MC}}$ from a CASSCF diabatization and $\mathbf{B}^{\mathrm{CD}}$ from a (X)MC-QDPT, to calculate $\mathbf{B}^{\mathrm{MD}}$ and uses Eq. (14) to calculate the diabatic potential energy matrix $\mathbf{U}$. The signs of the matrix elements of $\mathbf{B}^{\mathrm{MC}}$ and $\mathbf{B}^{\mathrm{CD}}$ are affected by the phases of the many-electron wave functions involved in the transformations. Whereas the phases of the diabatic states (affecting the signs of the columns of $\mathbf{B}^{\mathrm{CD}}$) and of the (X)MC-QDPT model states (affecting the signs of the rows of $\mathbf{B}^{\mathrm{MC}}$) are not important since they influence eventually only the signs of the off-diagonal elements of $\mathbf{U}$ (diabatic couplings), the phases of the CASSCF adiabatic states are critical and must be consistent in $\mathbf{B}^{\mathrm{MC}}$ and $\mathbf{B}^{\mathrm{CD}}$; otherwise we would get an incorrect $\mathbf{B}^{\mathrm{MD}}$ (the mathematical details behind this statement are given in the Appendix). Unfortunately, standard implementations of the methods do not automatically generate phases that are consistent between the (X)MC-QDPT part of the calculation (giving $\mathbf{B}^{\mathrm{MC}}$) and the fourfold way part of the calculation (giving $\mathbf{B}^{\mathrm{CD}}$); nor do they generate phases consistent from point to point in coordinate space. Nevertheless, we do not need uniquely defined phases; we only need the phases to be consistent. For systems with an even number of electrons, we are able to ensure this by examining their CAS-CI coefficients.

We note that the signs of the CSFs and thus of the CAS-CI coefficients can also be arbitrary because of the undetermined phases of the orbitals, with the important exception that closed-shell singlet CSFs with all occupied orbitals being doubly occupied are unaffected by the signs of orbitals, and the signs of their CAS-CI coefficients are determined by the overall phase of the wave function only. We used this exception in the scheme we used in this paper, taking advantage of the fact that all systems considered in this paper have an even number of electrons. For such systems, we can determine the phases of the CASSCF states in the (X)MC-QDPT and fourfold way calculations by the sign of the CAS-CI coefficient of a closed-shell CSF, and we can then adjust the signs of the rows of $\mathbf{B}^{\mathrm{CD}}$ so that it is consistent with $\mathbf{B}^{\mathrm{MC}}$. After attaining consistency between $\mathbf{B}^{\mathrm{MC}}$ and $\mathbf{B}^{\mathrm{CD}}$ at one geometry, we can enforce the smoothness of the two matrices at all geometries as a convenient way to ensure that $\mathbf{B}^{\mathrm{MC}}$ and $\mathbf{B}^{\mathrm{CD}}$ are also consistent in phase for those geometries. Based on this analysis, the scheme we used to adjust the signs of the elements of $\mathbf{B}^{\mathrm{MC}}$ and $\mathbf{B}^{\mathrm{CD}}$ so that they are consistent in the phases of the CASSCF states and across the molecular geometry space of interest is as follows.

(1) Choose a molecular geometry where DMOs are close to CMOs and find the CASSCF wave functions and their CAS-CI coefficients.
(2) Choose a certain CSF with all occupied orbitals doubly occupied, for example, the ground-state closed-shell CSF. Examine its CAS-CI coefficient for each state, whose sign is used as the "indicator" of the phase of that state. Note that in the diabatization output, the CSFs are in the DMO basis and their coefficients are different from those in the CMO basis in the (X)MC-QDPT output. However, they will be close when DMOs are close to CMOs.
(3) If for the $i$th CASSCF state the sign of the "indicator" coefficient is different in the fourfold way and (X)MC-QDPT, then change the signs of all elements of the $i$th row of $\mathbf{B}^{\mathrm{CD}}$. This adjustment will account for the different phases of the $i$th CASSCF state in the two calculations. Do this for all the CASSCF states.
(4) The matrix $\mathbf{B}^{\mathrm{CD}}$, adjusted according to the steps above, now becomes a reference for nearby geometries. At such adjacent geometries, the signs of the matrix elements of $\mathbf{B}^{\mathrm{MC}}$ and $\mathbf{B}^{\mathrm{CD}}$ are determined as follows. By changing the signs of any rows and columns of the matrices at the current geometry in all possible ways, we maximize an overlap-like function $M$ for $\mathbf{B}^{\mathrm{MC}}$ and $\mathbf{B}^{\mathrm{CD}}$, respectively,

$$M = \sum_{i,j} B_{ij}^{(\mathrm{ref})} B_{ij}^{(\mathrm{curr})}, \tag{15}$$

where $B_{ij}$ are elements of matrix $\mathbf{B}$, which is either $\mathbf{B}^{\mathrm{MC}}$ or $\mathbf{B}^{\mathrm{CD}}$; the sum is over all matrix elements; superscripts "ref" or "curr" mean the matrix is for the reference or current geometry. The current geometry is then used as the new reference and the matrices for the next adjacent geometry are adjusted in the same manner. We can follow a path of geometries and repeat this step for all geometries

of interest. This is equivalent to enforcing the smoothness of the transformation matrices across the geometries, which is more efficient than applying steps (1)-(4) at each geometry individually. Of course, one can use steps (1)-(4) to check the results if needed. The path to follow can be general; for example, it can encircle a conical intersection, in which case the adiabatic wave functions change sign due to the geometric phase effect[52] while the diabatic wave functions do not.

The procedure of ensuring the consistency in the phases of matrices across different geometries is applicable to any system. However, the procedure used here for making the phases of CASSCF wave functions consistent in $\mathbf{B}^{\mathrm{MC}}$ and $\mathbf{B}^{\mathrm{CD}}$ at a given geometry is limited to systems with an even number of electrons since it utilizes the CI coefficients of a singlet CSF with all occupied orbitals being doubly occupied; there is no such CSF for systems with an odd number of electrons. For open shell systems, one practically convenient alternative is to try all possible combinations of the phases of CASSCF wave functions in $\mathbf{B}^{\mathrm{MC}}$ and $\mathbf{B}^{\mathrm{CD}}$ and generate a set of diabatic potential energy curves for each combination of phases following a path while ensuring the consistency across the path. By looking at the sets of potential energy curves, one should be able to select the correct one, because the curves generated with consistent phases should be smooth and reflect the different positions of state crossings in the CASSCF-level and (X)MC-QDPT-level diabatizations. This procedure is convenient due to the fact that there are only a limited number of combinations of phases ($2^{N-1}$ combinations for a model space of dimension $N$ where $N$ is usually a small number in practical calculations of coupled potential energy surfaces) and that the procedure of generating diabatic potential energy curves using MSD is very efficient without the need of additional electronic structure calculations. More efficient schemes can probably be devised, but they will probably be software dependent.

## III. COMPUTATIONAL DETAILS

All SA-CASSCF, fourfold-way diabatizations, and XMC-QDPT calculations were carried out with the GAMESS[51] software package. Intruder state avoidance[53] for XMC-QDPT was used throughout with the energy denominator shift parameter[51] set equal to 0.02. The model space diabatization strategy was performed, using in-house developed codes, to extract the needed information from the outputs of the CASSCF diabatization and XMC-QDPT calculations, to adjust the phases of the matrices, and to calculate the diabatic potential energy matrices. The strategy was applied to the potential energy surfaces of three molecules: LiH, LiF, and thioanisole. The fourfold way at the XMC-QDPT level was also performed, with CASSCF DMOs in all cases, on these molecules for comparison.

The potential energy curves of the three lowest $^1\Sigma^+$ states of LiH were calculated with SA-CASSCF averaging over the three states with equal weights, and with XMC-QDPT with a three-dimensional model space, for internuclear distances from 1.5 to 6.0 Å. The coordinate system is defined by putting Li at the origin and H on the positive $z$ axis. The active space consists of two electrons in five orbitals, which have the character of $2s$ and $2p_z$ of Li and $1s$, $2p_x$, and $2p_y$ of H. Further increase of the active space results in no qualitative difference in the potential energy curves. The basis set used was aug-cc-pVDZ.[54] The SA-CASSCF calculations were constrained to $A_1$ states in $C_{4v}$ spatial symmetry. The XMC-QDPT calculations were carried out with $C_1$ spatial symmetry.

The potential energy curves of LiH were diabatized using the fourfold way. The threefold density criterion with parameters $\alpha_N = 2$, $\alpha_R = 1$, and $\alpha_T = 0.5$ is sufficient to generate satisfactory DMOs. The diabatic prototypes include one CSF for each state, corresponding nominally to configurations $(1s_H)^2$, $(1s_H)(1s_{Li})$, and $(1s_H)(1p_{z,Li})$.

The potential energy curves of the three lowest $^1\Sigma^+$ states of LiF were calculated with SA-CASSCF by averaging over the three states with equal weights, and with XMC-QDPT with a three-dimensional model space, for internuclear distances from 3.0 to 8.0 Å. The coordinate system is defined by putting Li at the origin and F on the positive $z$ axis. In $C_{2v}$ spatial symmetry, the active space consists of two electrons in eight orbitals, which have the character of one $s$ and one $p_y$ on Li and one $s$, one $p_y$, two $p_x$, and two $p_z$ on F. (Here, the labeling of $x$ and $y$ is arbitrary and interchangeable; notice, however, that the $C_{2v}$ symmetry does not treat the degenerate $x$ and $y$ components of the $\pi$ space equivalently.) Further increase of the active space results in no qualitative difference in the potential energy curves. The basis set used was aug-cc-pVTZ.[54,55] The SA-CASSCF and XMC-QDPT calculations were constrained to $A_1$ states in $C_{2v}$ spatial symmetry.

The potential energy curves of LiF were diabatized using the fourfold way. The threefold density criterion with parameters $\alpha_N = 2$, $\alpha_R = 1$, and $\alpha_T = 0.5$ is sufficient to generate satisfactory DMOs. The diabatic prototypes include one CSF for each state, corresponding nominally to three configurations: closed-shell $Li^+F^-$, excitation $(p_{z,F}) \rightarrow (s_{Li})$ from the closed shell, and excitation $(p_{y,F}) \rightarrow (p_{y,Li})$ from the closed shell.

The geometry of thioanisole was first optimized by density functional theory with the M06-2X exchange-correlation functional[56,57] and the MG3S basis set[58] using the *Gaussian* 09[59] software package. The optimized geometry has $C_s$ symmetry, and the coordinate system is defined by taking the symmetry plane as the $xy$ plane with the Ph-S bond on the $x$ axis. The potential energy curves of the three lowest singlet states of thioanisole, which are two A′ and one A″ states, were calculated along the S–$CH_3$ bond distance coordinate from 1.8 to 4.0 Å while other coordinates were fixed at their values at the equilibrium geometry, with SA-CASSCF averaging over the three states with equal weights and XMC-QDPT having a three-dimensional model space. The active space consists of 14 electrons in 13 orbitals, which have the character of three $\pi$ and three $\pi^*$ orbitals on the phenyl ring, one $\sigma$ and one $\sigma^*$ orbital on the Ph–S bond, one $\sigma$ and one $\sigma^*$ orbital on the S–$CH_3$ bond, and one $s$, one $p_z$, and one $d$ orbital on the sulfur. (The $d$ orbital is a combination of $d_{xz}$ and $d_{yz}$, and its orientation changes with the S–$CH_3$ distance.) The $\sigma$

and σ* canonical orbitals on the S–$CH_3$ bond become more localized when the diabatic orbitals are formed, as discussed below. The basis set used is a mixed one with 6-311+G(d)[60,61] for C and H and MG3S[58] for S. The SA-CASSCF and XMC-QDPT calculations were carried out in $C_1$ spatial symmetry.

The potential energy curves of thioanisole were diabatized using the fourfold way. The threefold density criterion with parameters $\alpha_N = 2$, $\alpha_R = 1$, and $\alpha_T = 0.5$ together with the MORMO criterion was used to generate DMOs. Two MORMO reference orbitals were used. One of them was prepared by taking a π CMO at $r_{S\text{-}CH_3} = 4.0$ Å and keeping its components in the atomic orbitals (AOs) of Ph–S and dropping the components in the AOs of $CH_3$. The other one was prepared by taking a sulfur $p_y$-like CMO and keeping its components in the AOs of sulfur only. (The shapes of the two reference orbitals are given in the supplementary material.[62]) With this choice of MORMO reference orbitals, the DMOs are close to CMOs except that at short S–$CH_3$ distances, the σ and σ* CMOs on the S–$CH_3$ bond become a $p_y$-like DMO on sulfur and a $sp^3$-like DMO on $CH_3$.

The selection of MORMO reference orbitals and diabatic prototypes is complicated because we chose them to be appropriate for calculating global potential energy surfaces, not just for the local cuts presented here. The diabatic prototypes are chosen as follows. For conciseness of description, we define a reference CSF corresponding to the closed-shell $[Ph–S]^-$ anion, with the bonding- and non-bonding-like DMOs on Ph-S doubly occupied (one $s$, one $p_y$, and one $p_z$ orbital on sulfur, three π orbitals on Ph, and one bonding orbital on the Ph-S bond) and the other anti-bonding-like orbitals on Ph–S and the $sp^3$-like orbital on $CH_3$ unoccupied. The prototype for the first state is one CSF corresponding to a single excitation from the $p_y$-like orbital on sulfur to the $sp^3$-like orbital on $CH_3$. Prototypes for the second state are three CSFs, two corresponding to single excitations from π to π*, and the other one corresponding to a double excitation from the $p_z$-like orbital on sulfur to a π* orbital on Ph-S and the $sp^3$-like orbital on $CH_3$. Prototypes for the third state are two CSFs, one corresponding to a single excitation from the $p_z$-like orbital on sulfur to the $sp^3$-like orbital on $CH_3$, the other corresponding to a single excitation from a π orbital to the $sp^3$-like orbital on $CH_3$.

## IV. RESULTS AND DISCUSSION

### A. LiH

The ionic-covalent crossing of LiH is a classic problem whose study dates back to the early days of quantum chemistry.[63,64] The lowest three $^1\Sigma^+$ states of LiH, denoted here as $V_1$, $V_2$, and $V_3$, are one ionic $[(1s_H)^2]$ and two covalent $[(1s_H)(2s_{Li}), (1s_H)(2p_{z,Li})]$ states. The adiabatic and diabatic potential energy curves given by SA-CASSCF and the fourfold way are shown in Fig. 3(a). The curve of $V_3$ is unsmooth at internuclear distance ~2.6 Å because it has an avoided crossing with a higher state, and it also affects $V_1$ and $V_2$ via state averaging. However, the higher state is not calculated since it has no significant influence on the diabatization. The ionic

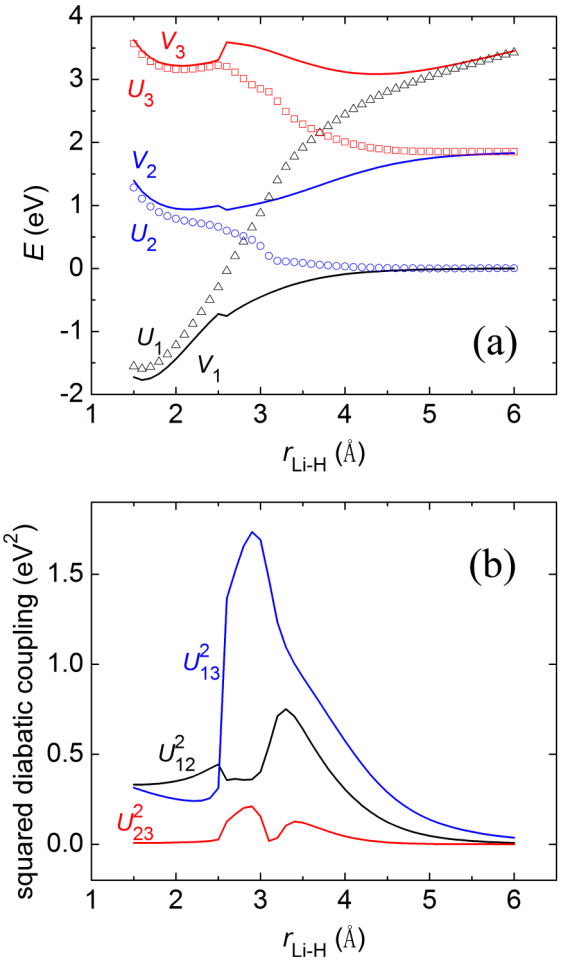


FIG. 3. Potentials and couplings for LiH as functions of the internuclear separation as calculated by SA-CASSCF and the fourfold way at the CASSCF level. (a) Adiabatic ($V_1 - V_3$; solid lines) and diabatic ($U_1 - U_3$; open symbols) potential energy curves and (b) the squared diabatic couplings $(U_{ij})^2$ between diabatic states $i$ and $j$ ($i$, $j$ = 1-3).

diabatic state $U_1$ transforms smoothly from adiabatic state $V_1$ near the equilibrium bond length of 1.595 Å (Ref. 65) to $V_3$ in the dissociation limit as the internuclear distance increases. The two covalent diabatic states $U_2$ and $U_3$ change from $V_2$ and $V_3$ at short bond lengths to $V_1$ and $V_2$, respectively, at the dissociation limit. There are two diabatic crossings, one at 2.8-2.9 Å between $U_1$ and $U_2$ and the other at ~3.7 Å between $U_1$ and $U_3$. The squared diabatic couplings shown in Fig. 3(b) are overall smooth except a small "kink" at $r_{Li\text{-}H} \sim 2.5$ Å caused by the sudden change of character of $V_3$. The couplings peak in the region where the diabatization mixes different adiabatic states and they decrease toward zero in the asymptotic region, as expected.

The adiabatic potential energy curves given by XMC-QDPT are shown in Fig. 4 together with the ones given by SA-CASSCF for comparison. The zero of energy for each theory is chosen to be the $S_0$ energy at $r_{Li\text{-}H} = 6.0$ Å given by that theory. The figure shows that XMC-QDPT deviates from SA-CASSCF significantly for $S_0$ at short bond lengths, for $S_1$ in the intermediate region, and for $S_2$ at the dissociation limit. This is because in those regions the particular adiabatic state has ionic character. The dynamic correlation introduced

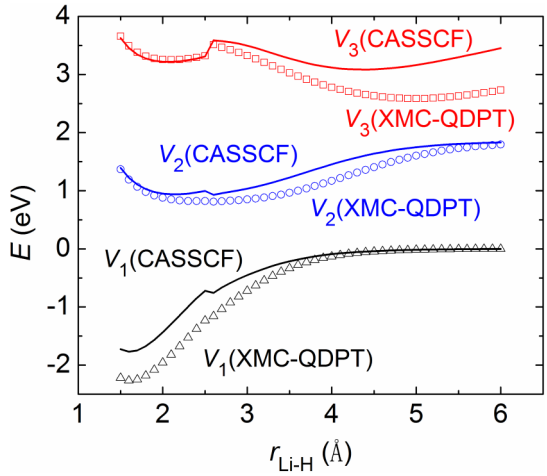


FIG. 4. Adiabatic ($V_1 - V_3$) potential energy curves of LiH as functions of the internuclear separation as calculated by SA-CASSCF (solid lines) and XMC-QDPT (open symbols). The zero of energy is set to be the ground-state energy at dissociation limit ($r_{\text{Li-H}} = 6.0$ Å) given by the respective theories.

by XMC-QDPT for the covalent states is similar for different internuclear distances, leading to an overall downshift of the absolute energies without significant effect on the relative energies, while the dynamic correlation for the ionic state is more pronounced, resulting in further lowering of the energies. Because of this, the diabatic crossing between the ionic and a covalent state should occur at different internuclear distances in SA-CASSCF and in XMC-QDPT. Such a difference has to be incorporated by the transformation $\mathbf{B}^{\text{MC}}$ that converts XMC-QDPT model states to CASSCF states since $\mathbf{B}^{\text{CD}}$, the transformation of CASSCF adiabatic states to diabatic states, has no information about this difference.

The XMC-QDPT-level diabatic potential energy curves given by the MSD strategy are shown in Fig. 5(a). The sign of $\mathbf{B}^{\text{CD}}$ has been adjusted for $r_{\text{Li-H}} = 1.5$ following steps (2)–(4) discussed in Sec. II C 3 as well as for all other $r_{\text{Li-H}}$ following step (5) to ensure the consistency of phases in $\mathbf{B}^{\text{MC}}$ and $\mathbf{B}^{\text{CD}}$ for each geometry and consistency over all geometries. The diabatic crossings occur at 3.0-3.1 Å between $U_1$ and $U_2$ and at 4.2-4.3 Å between $U_1$ and $U_3$, both at longer $r_{\text{Li-H}}$ compared to CASSCF. To emphasize the significance of phase consistency, diabatic potential energy curves obtained with inconsistent phases in $\mathbf{B}^{\text{MC}}$ and $\mathbf{B}^{\text{CD}}$ (but the individual matrices are smooth over different geometries) are also given in Figs. 5(b)–5(d) for comparison. (There are four possible combinations of the signs of rows in a 3×3 matrix $\mathbf{B}^{\text{CD}}$, with $\mathbf{B}^{\text{CD}}$ and $-\mathbf{B}^{\text{CD}}$ considered as the same, only one of which is consistent with a given $\mathbf{B}^{\text{MC}}$.) The diabatic curves in Figs. 5(b) and 5(d) are still smooth, but the shapes are incorrect. For instance, in Figs. 5(b) and 5(c), the crossing between $U_1$ and $U_3$ occurs at a similar position as for CASSCF diabatization, and the same happens for the

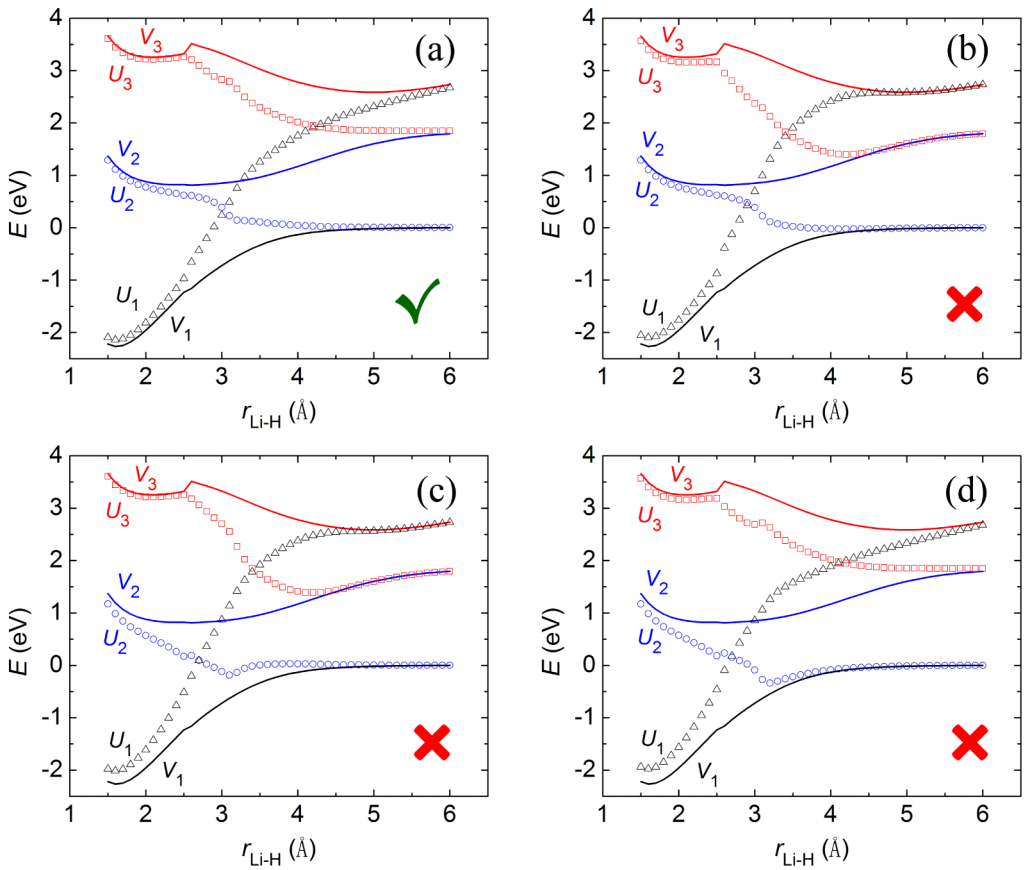


FIG. 5. Adiabatic ($V_1 - V_3$; solid lines) and diabatic ($U_1 - U_3$; open symbols) potential energy curves of LiH as functions of the internuclear separation as calculated by XMC-QDPT and the MSD strategy with transformation matrices corresponding to (a) consistent phases and ((b)–(d)) inconsistent phases of the wave functions. Only (a) is the proper result from the correct application of the MSD strategy (indicated by the check mark, as opposed to a red **x** for the other cases).

crossing between $U_1$ and $U_2$ in Fig. 5(d). The squared diabatic couplings shown in Fig. 6 corresponding to the diabatization in Fig. 5(a) are qualitatively similar to those at the CASSCF level in Fig. 3(b).

For this system, the DMOs generated by the threefold density criterion are close to CMOs, and as a result, the XMC-QDPT energies in the DMO basis differ only slightly from those in the CMO basis (mean unsigned deviation = 0.01 eV, maximum deviation = −0.03 eV); therefore, we have an additional check for the diabatic curves generated by the MSD strategy, namely, to compare them to those generated by the fourfold way at the XMC-QDPT level. Figure 7 shows they match well, further verifying the validity of the MSD strategy.

### B. LiF

The potential energy curves of the ground $X^1\Sigma^+$ and the excited $1^1\Sigma^+$ states of LiF also provide a challenging case for electronic structure methods because of their intrinsically multi-configurational character (usually called multireference character) when the bond stretches and because of the ionic-covalent avoided crossing[66,67] at internuclear distance $r_{\text{Li-F}} \sim 7.2$ Å.[67] On the left side of the avoided crossing where $r_{\text{Li-F}}$ is less than 7.2 Å, the $X^1\Sigma^+$ state has ionic character and the $1^1\Sigma^+$ state has covalent character, while the character of the two states switches on the other side of the crossing. Obtaining the correct distance for the avoided crossing depends on calculating the asymptotic energies of the ionic and covalent states accurately, and this requires a very high level calculation, especially for $F^-$. However, the present work is focused on diabatization methodology, not on obtaining a converged calculation of the crossing point. As for LiH, the ionic state of LiF is more sensitive than the covalent states to dynamic correlation, and SA-CASSCF and XMC-QDPT give significantly different locations of the ionic-covalent avoided crossings as discussed below. It therefore constitutes another difficult test case for MSD which utilizes information from diabatization at the CASSCF level to perform diabatization at the XMC-QDPT level.

The adiabatic and diabatic potential energy curves calculated by SA-CASSCF and the fourfold-way diabatization are shown in Fig. 8(a). The ionic diabatic state $U_1$ corresponds

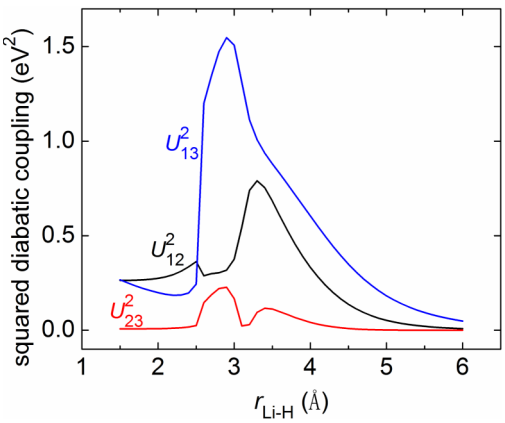


FIG. 6. Squared diabatic couplings $(U_{ij})^2$ between diabatic states $i$ and $j$ ($i$, $j$ = 1-3) of LiH as functions of the internuclear separation as calculated by the MSD strategy.

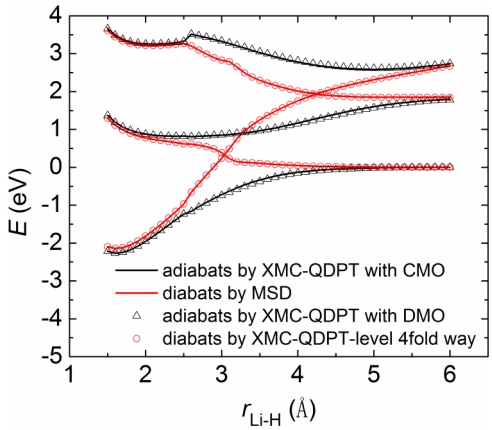


FIG. 7. Adiabatic and diabatic potential energy curves of LiH as functions of the internuclear separation. Black lines: adiabatic curves calculated by XMC-QDPT with CMOs. Red lines: diabatic curves calculated by MSD. Black triangles: adiabatic curves calculated by XMC-QDPT with CASSCF DMOs. Red circles: diabatic curves calculated by the fourfold way at the XMC-QDPT level with CASSCF DMOs.

to the adiabatic state $V_1$ at short Li-F distances, to $V_2$ at intermediate distances, and to $V_3$ at long distances, similar to LiH. The diabatic crossings occur at 4.1–4.2 Å between the ionic $U_1$ and covalent $U_2$ and at ~7.0 Å between $U_1$ and the covalent $U_3$. The squared diabatic couplings shown in Fig. 8(b)

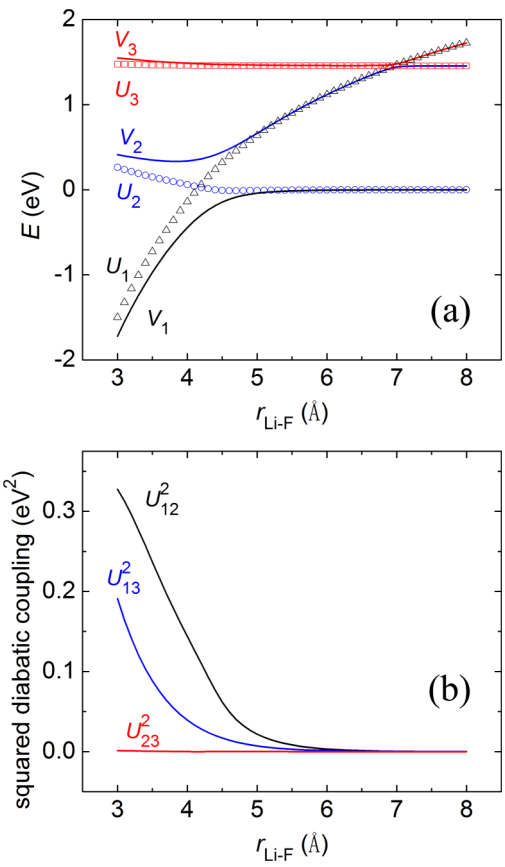


FIG. 8. Potentials and couplings for LiF as functions of the internuclear separation as calculated by SA-CASSCF and the fourfold way at the CASSCF level. (a) Adiabatic ($V_1 - V_3$; solid lines) and diabatic ($U_1 - U_3$; open symbols) potential energy curves; (b) the squared diabatic couplings $(U_{ij})^2$ between diabatic states $i$ and $j$ ($i$, $j$ = 1-3).

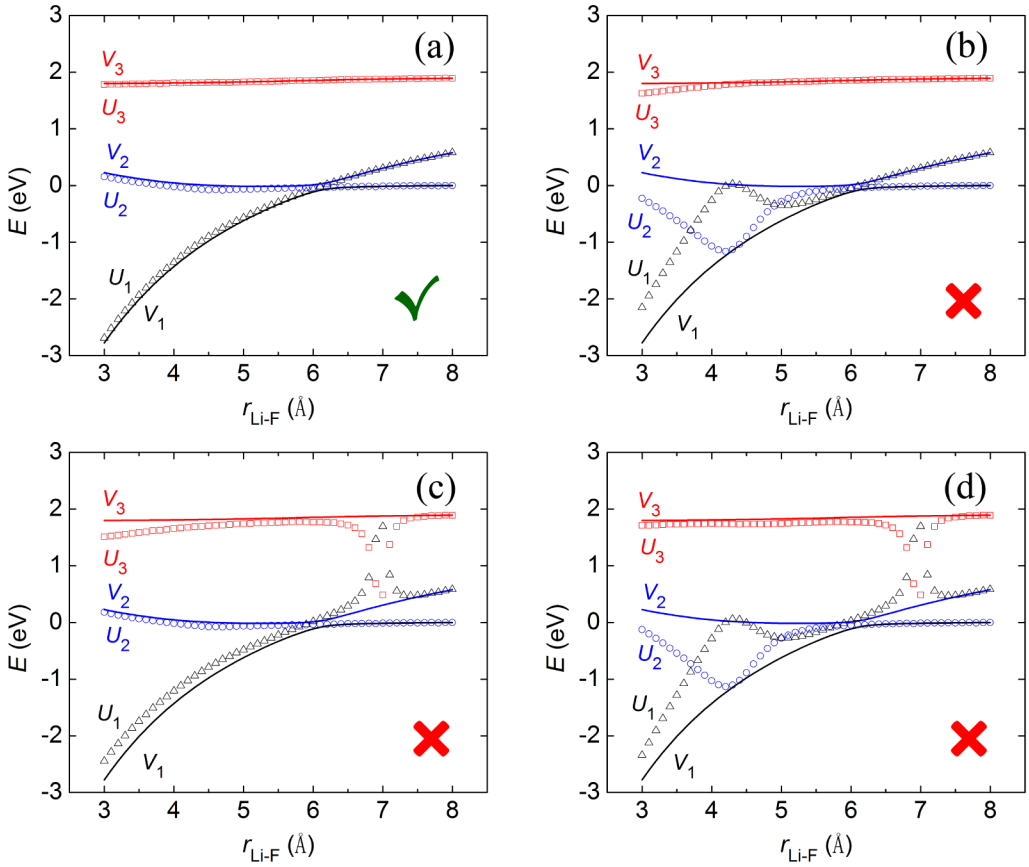


FIG. 9. Adiabatic ($V_1 - V_3$; solid lines) and diabatic ($U_1 - U_3$; open symbols) potential energy curves of LiF as functions of the internuclear separation as calculated by XMC-QDPT and the MSD strategy with transformation matrices corresponding to (a) consistent phases (indicated by a check mark) and ((b)–(d)) inconsistent phases (indicated by a red **x**) of the wave functions. Only the one with the check mark is the proper result from the correct application of the MSD strategy.

are again smooth and decrease toward zero in the asymptotic region.

The XMC-QDPT adiabatic and diabatic potential energy curves are shown in Fig. 9(a). The adiabatic curves are considerably different from the CASSCF ones due to the significantly different amounts of dynamic correlation for different states and at different geometries. As a consequence, the avoided crossing between $S_0$ and $S_1$ occurs at much longer $r_{Li-F}$, and the avoided crossing between $S_1$ and $S_2$ vanishes in the calculated bond distance range. These differences are fully captured by the MSD strategy. The resulting diabatic potential energy curves have only one crossing at ~6.1 Å between $U_1$ and $U_2$. Like what we have done for LiH, the diabatic curves of LiF generated from inconsistent $\mathbf{B}^{MC}$ and $\mathbf{B}^{CD}$ are shown in Figs. 9(b)–9(d). It is even more obvious here that the consistency of phase is essential for the correct diabatization, otherwise the diabatic curves will exhibit erratic shapes. (There are exceptions for which the phase is practically unimportant, to be discussed in Subsection IV C.) The squared diabatic couplings, shown in Fig. 10(a), have small bumps at ~4.5 Å and ~7.1 Å but the curves are still overall smooth. We note that the bumps originate from the fourfold way rather than the MSD strategy, as explained in the following.

As for LiH, the DMOs are also similar to CMOs for LiF and so the XMC-QDPT energies in the DMO basis are essentially the same as the standard XMC-QDPT energies in the CMO basis. Consequently, the fourfold way at the XMC-QDPT level is in principle equivalent to MSD. Indeed, they give essentially the same diabatic potential curves, differing by less than 0.01 eV (not shown here). The squared diabatic couplings (Fig. 10) given by the two schemes are also essentially the same despite some numerical differences. Obviously, the bumps at ~4.5 Å and ~7.1 Å are also present in the curves given by the fourfold way at the XMC-QDPT level (Fig. 10(b)), showing that it is not an inaccuracy introduced by MSD. Nonetheless, this "unsmoothness" is minor without noticeable influence on the potential energy curves and should not be a problem.

To test the sensitivity of the MSD strategy to using a model space of a different dimension, calculations were also carried out by SA-CASSCF averaging over only two states (again with equal weights) and with a two-dimensional model space for XMC-QDPT. The computational details and results are reported in the supplementary material.[62] The conclusions about the success of the MSD strategy are unchanged.

### C. Thioanisole

Thioanisole has 66 electrons, which is rather larger than is typical for a system used for testing new methods. We chose it because the use of MORMO reference orbitals in fourfold-way diabatization results in DMOs that are significantly

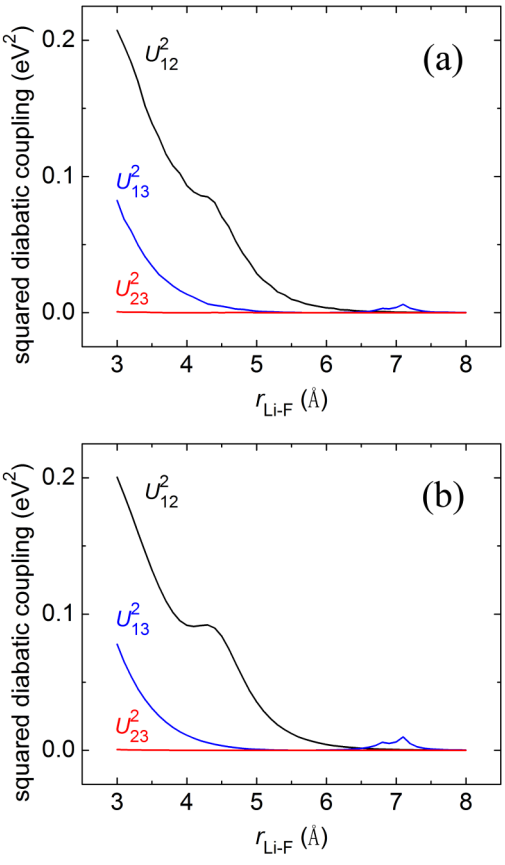


FIG. 10. Potentials and couplings of LiF as functions of the internuclear separation as calculated by MSD. (a) Squared diabatic couplings $(U_{ij})^2$ between diabatic states $i$ and $j$ ($i$, $j$ = 1-3) and (b) the fourfold way at the XMC-QDPT level with CASSCF DMOs.

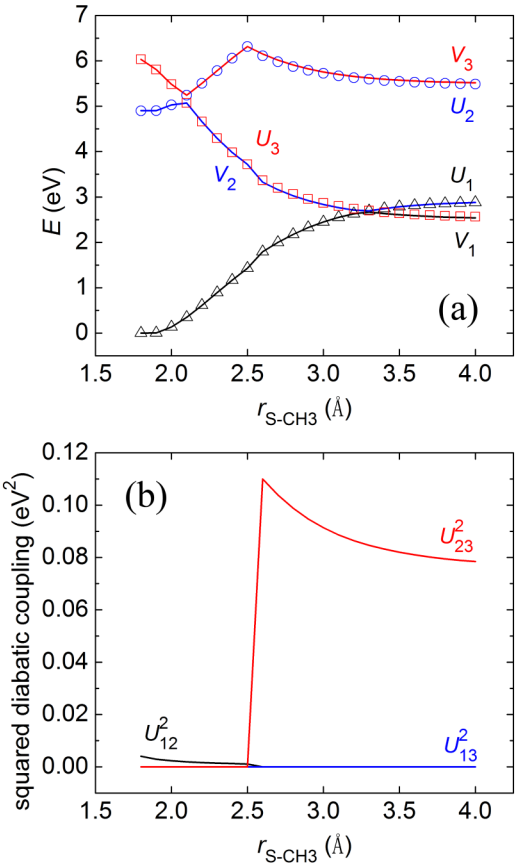


FIG. 11. Potentials and couplings for thioanisole along the S - $CH_3$ distance with the other coordinates fixed at the $S_0$ equilibrium geometry, as calculated by SA-CASSCF and the fourfold way at the CASSCF level. (a) Adiabatic ($V_1 - V_3$; solid lines) and diabatic ($U_1 - U_3$; open symbols) potential energy curves. (b) Squared diabatic couplings $(U_{ij})^2$ between diabatic states $i$ and $j$ ($i$, $j$ = 1-3).

different from CMOs, such that XMC-QDPT in the CASSCF DMO basis gives inaccurate energies, making the original MC-QDPT diabatization scheme[19,29] unsuitable. (The comparison of potential energy curves obtained by XMC-QDPT in the CMO and DMO bases is given in the supplementary material.[62])

At the equilibrium geometry of thioanisole, the ground state $S_0$ and the first excited singlet state $S_1$ belong to the A′ irreducible representation (irrep) in the $C_s$ group, while the second excited singlet state $S_2$ belongs to A″. $S_0$ is a closed-shell state, $S_1$ is a ππ* state, and $S_2$ is an nπ* state. Within $C_s$ symmetry, as the distance, $r_{\text{S-CH}_3}$, between sulfur and $CH_3$ increases, a symmetry-allowed conical intersection occurs first between $S_1$ and $S_2$. After this intersection, $S_1$ becomes an A″ state, and the second intersection occurs between $S_1$ and $S_0$ at longer $r_{\text{S-CH}_3}$. The intersections can be seen in the CASSCF adiabatic and diabatic potential energy curves in Fig. 11(a), located at $r_{\text{S-CH}_3}$ = 2.0–2.1 Å and ~3.3 Å. The crossing states should not mix in diabatization since they belong to different irreps, and the diabatic energies essentially overlap with the adiabatic ones. The diabatic states simply connect different adiabatic states as they pass the intersections so that $U_1$ and $U_2$ remain A′ states and $U_3$ remains an A″ state. The squared diabatic couplings, shown in Fig. 11(b), are overall small. $U_{23}$ undergoes an abrupt increase at $r_{\text{S-CH}_3}$ = 2.5 Å because $V_3$ passes another crossing (with the uncalculated $V_4$) and acquires a major configuration shared by $V_1$ so that the fourfold way distinguishes the two states less well. The coupling is nevertheless unimportant since its magnitude is still far smaller than the energy gap between the two states. At the XMC-QDPT level, the intersections occur at different locations, $r_{\text{S-CH}_3}$ = 1.9-2.0 Å and ~3.5 Å, due to the inclusion of dynamical correlation (Fig. 12(a)). The diabatic potential energies again match the adiabatic ones, and the difference of location of the intersections is properly reflected. The fact that the CASSCF diabatic wave functions are essentially the same as the adiabatic wave functions means that $\mathbf{B}^{\text{CD}}$ serves only to map the adiabatic states to diabatic states one-to-one with virtually no mixing, and as a consequence, the phase inconsistency is not a problem since it affects only the mixing of states. (All four possible phase choices of $\mathbf{B}^{\text{CD}}$ give essentially the same diabatic curves, which are not shown individually.) Diabatization at the XMC-QDPT level again introduces a minor unsmoothness to the squared diabatic couplings in Fig. 12(b) compared to Fig. 11(b), but the couplings are so small that the lack of smoothness is insignificant.

## V. SUMMARY

We have proposed a diabatization strategy called model space diabatization that, when used with an MCSCF-level

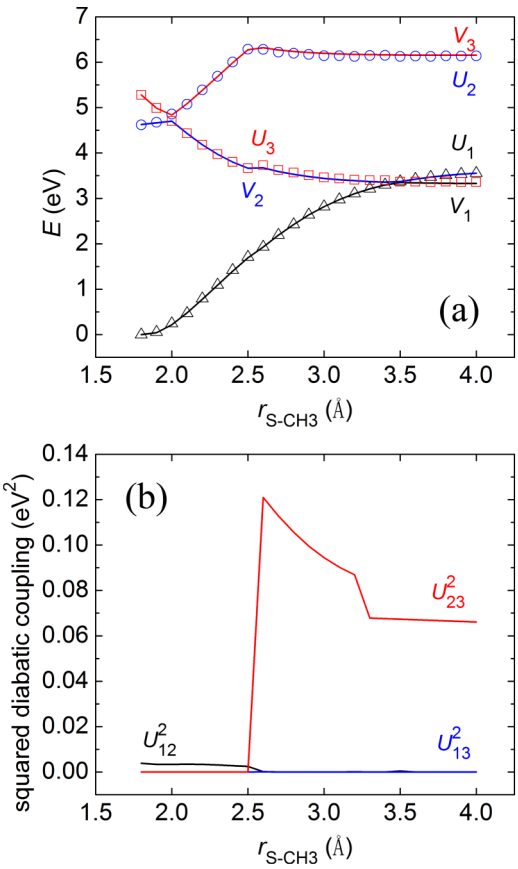


FIG. 12. Potentials and couplings for thioanisole along the S - $CH_3$ distance with the other coordinates fixed at the $S_0$ equilibrium geometry, as calculated by XMC-QDPT and the MSD strategy. (a) Adiabatic ($V_1 - V_3$; solid lines) and diabatic ($U_1 - U_3$; open symbols) potential energy curves. (b) Squared diabatic couplings $(U_{ij})^2$ between diabatic states $i$ and $j$ ($i$, $j$ = 1-3).

diabatization and a QDPT post-SCF method, generates diabatic states and diabatic potential energy matrix at the standard QDPT level. Diagonalizing the diabatic potential energy matrix produced by model space diabatization gives states and energies that agree exactly with the usual adiabatic states and energies.

The new diabatization method has been applied with the fourfold-way SA-CASSCF-level diabatization and XMC-QDPT adiabatic energies to obtain diabatic potential energy curves for LiH and LiF and cuts through the diabatic potential energy surfaces for thioanisole. These cases provide a critical challenge to the new method because the shape of the potential energy curves at the XMC-QDPT level is qualitatively different from those at the SA-CASSCF level for these molecules as a result of the inclusion of dynamic correlation; in particular, the avoided crossings or conical intersections occur at different geometries according to the two levels of theory. We find that these differences are properly accounted for by the MSD method, and the resulting diabatic potential energy curves are smooth with the correct shape.

The original fourfold way for QDPT calculations used DMOs determined at the QDPT level.[19] We have now made two changes. First, in a previous paper,[29] we showed that the method could be used, even for QDPT calculations, with DMOs determined at the CASSCF level. Second, in the present paper, we show that it can be used, even for QDPT calculations, with an adiabatic-to-diabatic transformation determined at the CASSCF level; this preserves the accuracy of the QDPT adiabatic energies even when the DMOs differ largely from the canonical molecular orbitals. With these two changes, the method becomes more convenient and more general. Although we have mainly discussed MSD as an extension of the fourfold way, it is also a general scheme that can, in principle, be used with any other MCSCF-level diabatization scheme that produces diabatic states spanning the same space as do the MCSCF adiabatic states. Furthermore, it can be used with any QDPT method that produces model states spanning the same space.

The MSD strategy is simple in that it can be applied as an independent step after the MCSCF diabatization calculations and QDPT calculations are finished, and its use does not require one to modify the electronic structure codes; furthermore, the additional computational cost is negligible. With these advantages, the strategy is recommended for QDPT-level diabatization of potential energy surfaces involving avoided crossings or conical intersections.

## ACKNOWLEDGMENTS

The authors are grateful to Xuefei Xu and Ke R. Yang for many helpful discussions and to Alex Granovsky for email discussions of QDPT. This work was supported in part (S.L.L. and D.G.T.) by the U.S. Department of Energy, Office of Basic Energy Sciences, under Grant No. DE-SC0008666. S.L.L. was also supported by the Dr. V. Pothapragada Excellence Fellowship in Chemistry, University of Minnesota. M.W.S. and M.S.G. were supported by the Air Force Office of Scientific Research under AFOSR Award No. FA9550-11-1-0099.

## APPENDIX: HOW THE PHASES OF WAVE FUNCTIONS AFFECT THE MSD STRATEGY

### 1. The relation between the phases of wave functions and the signs of rows and columns of a transformation matrix

To be concrete, let us consider the transformation matrix $\mathbf{B}^{\mathrm{CM}}$ converting CASSCF states to (X)MC-QDPT model states for a two-state problem (with two-dimensional model space) as an example. Suppose a valid relation is

$$\begin{pmatrix}\mathbf{c}_1 & \mathbf{c}_2\end{pmatrix}\begin{pmatrix}B^{\mathrm{CM}}_{11} & B^{\mathrm{CM}}_{12}\\ B^{\mathrm{CM}}_{21} & B^{\mathrm{CM}}_{22}\end{pmatrix}=\begin{pmatrix}\mathbf{m}_1 & \mathbf{m}_2\end{pmatrix}, \tag{A1}$$

where bold-faced letters denote CAS-CI vectors, in particular $\mathbf{c}_1$ and $\mathbf{c}_2$ are CASSCF states, and $\mathbf{m}_1$ and $\mathbf{m}_2$ are model states. If $\mathbf{c}_i$ changes its sign, the $i$th row of $\mathbf{B}^{\mathrm{CM}}$ has to change sign accordingly; e.g., for $i = 2$,

$$\begin{pmatrix}\mathbf{c}_1 & -\mathbf{c}_2\end{pmatrix}\begin{pmatrix}B^{\mathrm{CM}}_{11} & B^{\mathrm{CM}}_{12}\\ -B^{\mathrm{CM}}_{21} & -B^{\mathrm{CM}}_{22}\end{pmatrix}=\begin{pmatrix}\mathbf{m}_1 & \mathbf{m}_2\end{pmatrix}. \tag{A2}$$

On the other hand, if $\mathbf{m}_i$ changes sign, the $i$th column of $\mathbf{B}^{\mathrm{CM}}$ has to change sign accordingly; e.g. for $i = 2$,

$$\begin{pmatrix}\mathbf{c}_1 & \mathbf{c}_2\end{pmatrix}\begin{pmatrix}B^{\mathrm{CM}}_{11} & -B^{\mathrm{CM}}_{12}\\ B^{\mathrm{CM}}_{21} & -B^{\mathrm{CM}}_{22}\end{pmatrix}=\begin{pmatrix}\mathbf{m}_1 & -\mathbf{m}_2\end{pmatrix}. \tag{A3}$$

Apparently, this applies to any $N$ by $N$ transformation. We conclude that the signs of the rows of a transformation are related to the phases of the states *to be transformed*, while the signs of the columns are related to the phases of the *transformed* states.

### 2. The effect of the phases of the transformation matrices on the calculation of the diabatic potential energy matrix

To see how the signs of the elements of the transformation matrices affect the calculation of the diabatic potential energy matrix $\mathbf{U}$, we note first that changing the signs of some rows of a matrix $\mathbf{B}$ is equivalent to left-multiplying it by a diagonal matrix whose diagonal element is $-1$ if the corresponding row is to change sign or 1 if otherwise, e.g.,

$$\begin{pmatrix} B_{11} & B_{12} \\ -B_{21} & -B_{22} \end{pmatrix} = \begin{pmatrix} 1 & 0 \\ 0 & -1 \end{pmatrix} \begin{pmatrix} B_{11} & B_{12} \\ B_{21} & B_{22} \end{pmatrix}. \tag{A4}$$

Changing the signs of some columns of a matrix $\mathbf{B}$ is equivalent to right-multiplying it by a diagonal matrix whose diagonal element is $-1$ if the corresponding column is to change sign or 1 if otherwise, e.g.,

$$\begin{pmatrix} B_{11} & -B_{12} \\ B_{21} & -B_{22} \end{pmatrix} = \begin{pmatrix} B_{11} & B_{12} \\ B_{21} & B_{22} \end{pmatrix} \begin{pmatrix} 1 & 0 \\ 0 & -1 \end{pmatrix}. \tag{A5}$$

Therefore, we can account for the sign changes of the rows and columns of a matrix by left- and right-multiplying it by such matrices which we will denote as $\mathbf{J}$,

$$J_{ij} = (-1)^{\alpha_i} \delta_{ij}, \tag{A6}$$

where $\alpha_i = 0$ or 1, $\delta_{ij}$ is the Kronecker delta function. Different $\mathbf{J}$ matrices commute. Each $\mathbf{J}$ matrix satisfies the following equality:

$$\mathbf{J}^{\mathrm{T}} = \mathbf{J}^{-1} = \mathbf{J}, \tag{A7}$$

where superscripts "T" and "$-1$" denote transpose and inverse, respectively.

Now let us assume that a $\mathbf{B}^{\mathrm{MC}}$ and a $\mathbf{B}^{\mathrm{CD}}$ corresponding to consistent choices of phase for the wave functions have been found, and the following relation is valid (equivalent to Eq. (14)):

$$\mathbf{U} = \left(\mathbf{B}^{\mathrm{CD}}\right)^{\mathrm{T}} \left(\mathbf{B}^{\mathrm{MC}}\right)^{\mathrm{T}} \mathbf{V} \mathbf{B}^{\mathrm{MC}} \mathbf{B}^{\mathrm{CD}}. \tag{A8}$$

However, the matrices printed by electronic structure calculations, denoted as $\tilde{\mathbf{B}}^{\mathrm{MC}}$ and $\tilde{\mathbf{B}}^{\mathrm{CD}}$, may differ from the ones above by the signs of rows and columns. Using the $\mathbf{J}$ matrices, we can write in general

$$\tilde{\mathbf{B}}^{\mathrm{MC}} = \mathbf{J}_{\mathrm{r}}^{\mathrm{MC}} \mathbf{B}^{\mathrm{MC}} \mathbf{J}_{\mathrm{c}}^{\mathrm{MC}}, \quad \tilde{\mathbf{B}}^{\mathrm{CD}} = \mathbf{J}_{\mathrm{r}}^{\mathrm{CD}} \mathbf{B}^{\mathrm{CD}} \mathbf{J}_{\mathrm{c}}^{\mathrm{CD}}, \tag{A9}$$

where the subscripts "r" and "c" of the $\mathbf{J}$ matrices signify that they are responsible for the sign change of rows and columns, respectively. Using these matrices, the calculated diabatic potential energy matrix is

$$\begin{aligned} \tilde{\mathbf{U}} &= \left(\tilde{\mathbf{B}}^{\mathrm{CD}}\right)^{\mathrm{T}} \left(\tilde{\mathbf{B}}^{\mathrm{MC}}\right)^{\mathrm{T}} \mathbf{V} \tilde{\mathbf{B}}^{\mathrm{MC}} \tilde{\mathbf{B}}^{\mathrm{CD}} \\ &= \mathbf{J}_{\mathrm{c}}^{\mathrm{CD}} \left(\mathbf{B}^{\mathrm{CD}}\right)^{\mathrm{T}} \mathbf{J}_{\mathrm{r}}^{\mathrm{CD}} \mathbf{J}_{\mathrm{c}}^{\mathrm{MC}} \left(\mathbf{B}^{\mathrm{MC}}\right)^{\mathrm{T}} \mathbf{J}_{\mathrm{r}}^{\mathrm{MC}} \mathbf{V} \mathbf{J}_{\mathrm{r}}^{\mathrm{MC}} \mathbf{B}^{\mathrm{MC}} \mathbf{J}_{\mathrm{c}}^{\mathrm{MC}} \mathbf{J}_{\mathrm{r}}^{\mathrm{CD}} \mathbf{B}^{\mathrm{CD}} \mathbf{J}_{\mathrm{c}}^{\mathrm{CD}}. \end{aligned} \tag{A10}$$

Our aim is to analyze the effect of the $\mathbf{J}$ matrices on the calculated $\tilde{\mathbf{U}}$, compared to the $\mathbf{U}$ in Eq. (A8) that is correct by assumption.

The first observation is that $\mathbf{J}_{\mathrm{r}}^{\mathrm{MC}} \mathbf{V} \mathbf{J}_{\mathrm{r}}^{\mathrm{MC}} = \mathbf{V}$. It means the signs of the rows of $\tilde{\mathbf{B}}^{\mathrm{MC}}$, corresponding to the phases of the (X)MC-QDPT model states, have no consequence. Second, if we rewrite Eq. (A10) as

$$\mathbf{J}_{\mathrm{c}}^{\mathrm{CD}} \tilde{\mathbf{U}} \mathbf{J}_{\mathrm{c}}^{\mathrm{CD}} = \left(\mathbf{B}^{\mathrm{CD}}\right)^{\mathrm{T}} \mathbf{J}_{\mathrm{r}}^{\mathrm{CD}} \mathbf{J}_{\mathrm{c}}^{\mathrm{MC}} \left(\mathbf{B}^{\mathrm{MC}}\right)^{\mathrm{T}} \mathbf{J}_{\mathrm{r}}^{\mathrm{MC}} \mathbf{V} \mathbf{J}_{\mathrm{r}}^{\mathrm{MC}} \mathbf{B}^{\mathrm{MC}} \mathbf{J}_{\mathrm{c}}^{\mathrm{MC}} \mathbf{J}_{\mathrm{r}}^{\mathrm{CD}} \mathbf{B}^{\mathrm{CD}}, \tag{A11}$$

we see that $\mathbf{J}_{\mathrm{c}}^{\mathrm{CD}}$, responsible for the signs of columns of $\tilde{\mathbf{B}}^{\mathrm{CD}}$ and the phases of the diabatic states, only affects the signs of the off-diagonal elements of the diabatic potential energy matrix without changing its nature. The only significant part is the product of $\mathbf{J}_{\mathrm{c}}^{\mathrm{MC}}$ and $\mathbf{J}_{\mathrm{r}}^{\mathrm{CD}}$. The calculated $\tilde{\mathbf{U}}$ will be correct (differing from $\mathbf{U}$ only by the signs of off-diagonal elements) if and only if $\mathbf{J}_{\mathrm{c}}^{\mathrm{MC}} \mathbf{J}_{\mathrm{r}}^{\mathrm{CD}} = \pm \mathbf{I}$, where $\mathbf{I}$ is the identity matrix. This corresponds to the consistency of the phases of CASSCF wave functions used in the construction of the two matrices. One may keep $\mathbf{J}_{\mathrm{c}}^{\mathrm{MC}}$ intact and adjust $\mathbf{J}_{\mathrm{r}}^{\mathrm{CD}}$, equivalent to changing the signs of rows of $\tilde{\mathbf{B}}^{\mathrm{CD}}$, to satisfy the condition, which is what we adopted in this paper.


[1] A. W. Jasper, C. A. Kendrick, C. A. Mead, and D. G. Truhlar, in *Modern Trends in Chemical Reaction Dynamics: Experiment and Theory (Part 1)*, edited by X. Yang and K. Liu (World Scientific, Singapore, 2004), p. 329.
[2] L. S. Cederbaum, in *Conical Intersections: Electronic Structure, Dynamics and Spectroscopy*, edited by W. Domcke, D. R. Yarkony, and H. Köppel (World Scientific, Singapore, 2004), p. 3.
[3] W. Domcke and D. R. Yarkony, Annu. Rev. Phys. Chem. **63**, 325 (2012).
[4] B. C. Garrett and D. G. Truhlar, *in Theoretical Chemistry: Theory of Scattering: Papers in Honor of Henry Eyring*, edited by D. Henderson (Academic, New York, 1981), p. 215.
[5] C. A. Mead and D. G. Truhlar, J. Chem. Phys. **77**, 6090 (1982).
[6] W. Lichten, Phys. Rev. **131**, 229 (1963).
[7] A. Macias and A. Riera, J. Phys. B **11**, L489 (1978).
[8] J. B. Delos, Rev. Mod. Phys. **53**, 287 (1981).
[9] F. Spiegelmann and J. P. Malrieu, J. Phys. B **17**, 1259 (1984).
[10] V. Sidis, Adv. Chem. Phys. **82**, 73 (1992).
[11] R. Cimiraglia, in *Time-Dependent Quantum Molecular Dynamics*, edited by J. Broeckhoeve and L. Lathouwers (Plenum, New York, 1992), pp. 11–26.
[12] W. Domcke and C. Woywood, Chem. Phys. Lett. **216**, 362 (1993).
[13] K. Ruedenberg and G. J. Atchity, J. Chem. Phys. **99**, 3799 (1993).
[14] R. Thürwachter and P. Halvick, Chem. Phys. **221**, 33 (1997).
[15] G. J. Atchity and K. Ruedenberg, Theor. Chem. Acc. **97**, 47 (1997).
[16] D. Simah, B. Hartke, and H.-J. Werner, J. Chem. Phys. **111**, 4523 (1999).
[17] E. S. Kryachenko and D. R. Yarkony, Int. J. Quantum Chem. **76**, 235 (2000).
[18] H. Nakamura and D. G. Truhlar, J. Chem. Phys. **115**, 10353 (2001).
[19] H. Nakamura and D. G. Truhlar, J. Chem. Phys. **117**, 5576 (2002).
[20] M. P. Fülscher and L. Serrano-Andrés, Mol. Phys. **100**, 903 (2002).
[21] H. Nakamura and D. G. Truhlar, J. Chem. Phys. **118**, 6816 (2003).
[22] H. Köppel, in *Conical Intersections: Electronic Structure Dynamics and Spectroscopy*, edited by W. Domcke, D. R. Yarkony, and H. Köppel (World Scientific Publishing Co., Singapore, 2004), p. 175.
[23] O. Godsi, C. R. Evenhuis, and M. A. Collins, J. Chem. Phys. **125**, 104105 (2006).
[24] C. Mota and A. J. C. Varandas, J. Phys. Chem. A **112**, 3768 (2008).
[25] A. Cembran, L. Song, Y. Mo, and J. Gao, J. Chem. Theory Comput. **5**, 2702 (2009).
[26] R. Valero, L. Song, J. Gao, and D. G. Truhlar, J. Chem. Theory Comput. **5**, 1 (2009).
[27] T. Van Voorhis, T. Kowalczyk, B. Kaduk, L.-P. Wang, C.-L. Cheng, and Q. Wu, Annu. Rev. Phys. Chem. **61**, 149 (2010).
[28] A. J. Zhang, P.-Y. Zhang, T.-S. Chu, K.-L. Han, and G.-Z. He, J. Chem. Phys. **137**, 194305 (2012).
[29] K. R. Yang, X. Xu, and D. G. Truhlar, Chem. Phys. Lett. **573**, 84 (2013).
[30] C. E. Hoyer, X. Xu, D. Ma, L. Gagliardi, and D. G. Truhlar, J. Chem. Phys. **141**, 114104 (2014).

[31]W. Eisfeld, O. Vieuxmaire, and A. Viel, J. Chem. Phys. **140**, 224109 (2014).
[32]P. Siegbahn, A. Heiberg, B. Roos, and B. Levy, Phys. Scr. **21**, 323 (1980).
[33]J. Olsen, B. O. Roos, P. Jørgensen, and H. J. A. Jensen, J. Chem. Phys. **89**, 2185 (1988).
[34]H. Nakano and K. Hirao, Chem. Phys. Lett. **317**, 90 (2000).
[35]J. Ivanic, J. Chem. Phys. **119**, 9364 (2003).
[36]D. Ma, G. Li Manni, and L. Gagliardi, J. Chem. Phys. **135**, 044128 (2011).
[37]H. Nakano, J. Chem. Phys. **99**, 7983 (1993); Chem. Phys. Lett. **207**, 372 (1993).
[38]A. A. Granovsky, J. Chem. Phys. **134**, 214113 (2011).
[39]J. Finley, P.-Å. Malmqvist, B. O. Roos, and L. Serrano-Andrés, Chem. Phys. Lett. **288**, 299 (1998).
[40]C. Angeli, S. Borini, M. Cestari, and R. Cimiraglia, J. Chem. Phys. **121**, 4043 (2004).
[41]H. Nakano, R. Uchiyama, and K. Hirao, J. Comput. Chem. **23**, 1166 (2002); M. Miyajima, Y. Watanabe, and H. Nakano, J. Chem. Phys. **124**, 044101 (2006); R. Ebisuzaki, Y. Watanabe, and H. Nakano, Chem. Phys. Lett. **442**, 164 (2007); R. Ebisuzaki, Y. Watanabe, Y. Kawashima, and H. Nakano, J. Chem. Theory Comput. **7**, 998 (2011).
[42]T. Shiozaki, W. Győrffy, P. Celani, and H.-J. Werner, J. Chem. Phys. **135**, 081106 (2011).
[43]R. Valero and D. G. Truhlar, J. Chem. Phys. **125**, 194305 (2006).
[44]Z. H. Li, R. Valero, and D. G. Truhlar, Theor. Chem. Acc. **118**, 9 (2007).
[45]R. Valero and D. G. Truhlar, J. Phys. Chem. A **111**, 8536 (2007).
[46]R. Valero, D. G. Truhlar, and A. W. Jasper, J. Phys. Chem. A **112**, 5756 (2008).
[47]R. Valero and D. G. Truhlar, J. Chem. Phys. **137**, 22A539 (2012).
[48]X. Xu, K. R. Yang, and D. G. Truhlar, J. Chem. Theory Comput. **9**, 3612 (2013).
[49]C. Woywod, M. Stengle, W. Domcke, H. Flöthmann, and R. Schinke, J. Chem. Phys. **107**, 7282 (1997); D. Simah, B. Hartke, and H.-J. Werner, *ibid.* **111**, 4523 (1999).
[50]K. Hirao, Chem. Phys. Lett. **190**, 374 (1992); **196**, 397 (1992); Int. J. Quantum Chem. **44**(S26), 517 (1992).
[51]M. W. Schmidt, K. K. Baldridge, J. A. Boatz, S. T. Elbert, M. S. Gordon, J. H. Jensen, S. Koseki, N. Matsunaga, K. A. Nguyen, S. J. Su, T. L. Windus, M. Dupuis, and J. A. Montgomery, J. Comput. Chem. **14**, 1347 (1993); M. S. Gordon and M. W. Schmidt, in *Theory and Applications of Computational Chemistry: The First Forty Years*, edited by C. E. Dykstra, G. Frenking, K. S. Kim, and G. E. Scuseria (Elsevier, Amsterdam, 2005), pp. 1167–1189.
[52]C. A. Mead and D. G. Truhlar, J. Chem. Phys. **70**, 2284–2296 (1979); Erratum, **78**, 6344 (1983).
[53]H. A. Witek, Y.-K. Choe, J. P. Finley, and K. Hirao, J. Comput. Chem. **23**, 957 (2002).
[54]J. T. H. Dunning, J. Chem. Phys. **90**, 1007 (1989).
[55]R. A. Kendall, J. T. H. Dunning, and R. J. Harrison, J. Chem. Phys. **96**, 6796 (1992).
[56]Y. Zhao and D. G. Truhlar, Theor. Chem. Acc. **120**, 215 (2008).
[57]Y. Zhao and D. G. Truhlar, Acc. Chem. Res. **41**, 157 (2008).
[58]B. J. Lynch, Y. Zhao, and D. G. Truhlar, J. Phys. Chem. A **107**, 1384 (2003).
[59]G. W. T. M. J. Frisch, H. B. Schlegel, G. E. Scuseria, J. R. C. M. A. Robb, G. Scalmani, V. Barone, B. Mennucci, H. N. G. A. Petersson, M. Caricato, X. Li, H. P. Hratchian, J. B. A. F. Izmaylov, G. Zheng, J. L. Sonnenberg, M. Hada, K. T. M. Ehara, R. Fukuda, J. Hasegawa, M. Ishida, T. Nakajima, O. K. Y. Honda, H. Nakai, T. Vreven, J. A. Montgomery, Jr., F. O. J. E. Peralta, M. Bearpark, J. J. Heyd, E. Brothers, V. N. S. K. N. Kudin, T. Keith, R. Kobayashi, J. Normand, A. R. K. Raghavachari, J. C. Burant, S. S. Iyengar, J. Tomasi, N. R. M. Cossi, J. M. Millam, M. Klene, J. E. Knox, J. B. Cross, C. A. V. Bakken, J. Jaramillo, R. Gomperts, R. E. Stratmann, A. J. A. O. Yazyev, R. Cammi, C. Pomelli, J. W. Ochterski, K. M. R. L. Martin, V. G. Zakrzewski, G. A. Voth, J. J. D. P. Salvador, S. Dapprich, A. D. Daniels, J. B. F. O. Farkas, J. V. Ortiz, J. Cioslowski, and D. J. Fox, Gaussian 09, Revision C.01, Gaussian, Inc., Wallingford CT, 2010.
[60]R. Krishnan, J. S. Binkley, R. Seeger, and J. A. Pople, J. Chem. Phys. **72**, 650 (1980).
[61]T. Clark, J. Chandrasekhar, G. W. Spitznagel, and P. V. R. Schleyer, J. Comput. Chem. **4**, 294 (1983).
[62]See supplementary material at http://dx.doi.org/10.1063/1.4907038 for the MORMO reference orbitals used for the fourfold-way diabatization of thioanisole, for a comparison of the potential energy curves of thioanisole calculated by XMC-QDPT in the basis of CMOs and DMOs, and for the computational details and results of the two-state calculations for LiF.
[63]R. S. Mulliken, Phys. Rev. **50**, 1028 (1936).
[64]W. C. Stwalley and W. T. Zemke, J. Phys. Chem. Ref. Data **22**, 87 (1993).
[65]See http://cccbdb.nist.gov/expbondlengths2.asp?descript=rLiH&all=0 for the equilibrium bond length of LiH (accessed 3 October 2014).
[66]M. Hanrath, Mol. Phys. **106**, 1949 (2008).
[67]A. J. C. Varandas, J. Chem. Phys. **131**, 124128 (2009); **135**, 119902(E) (2011).